Modulating Stereoselectivity through Electrostatic Interactions in a SPINOL-Phosphoric Acid Catalyzed Synthesis of 2,3-Dihydroquinazolinones

Croix J. Laconsay,[‡a] Trevor J. Seguin,[‡b] and Steven E. Wheeler[‡§*]

[‡]*Department of Chemistry, Texas A&M University, College Station, TX 77842*
[§]*Department of Chemistry, University of Georgia, Athens, GA 30602*, USA

[*]*E-mail: swheele2@uga.edu*

Abstract

Chiral phosphoric acids have received considerable attention due to their excellent performance in many asymmetric catalytic reactions. However, the full breadth of means by which the stereoselectivity of these catalysts can be tuned has not been fully elucidated. Herein, the origin of enantioselectivity in a catalytic asymmetric synthesis of 2,3-dihydroquinazolinones (DHQZ's) using SPINOL-derived chiral phosphoric acids (*ACS Catal.* **2013**, *3*, 2244) is explored using density functional theory (DFT) computations. We show that the enantioselectivity of this reaction is determined during the intramolecular amine addition step of an organocascade sequence and is modulated by differential non-covalent interactions of the substrate with the aryl groups of the catalyst as well as CH···O and NH···O interactions with the phosphate core of the catalyst. Most notably, we demonstrate that the strength of these latter interactions is modulated by their position within the electrostatic environment created by the catalyst. This provides clear evidence of the ability to precisely control the selectivity of an organocatalyzed reaction through the tuning of electrostatic interactions.

Keywords: stereoselectivity; density functional theory; non-covalent interactions; chiral phosphoric acid; hydrogen bonding

[a] Present Address: Department of Chemistry, University of California, Davis, CA 95616
[b] Present Address: Lawrence Berkeley National Laboratory, Berkeley, CA 94720

I. Introduction

Brønsted-acid catalysts derived from chiral diols (chiral phosphoric acids, or CPAs) have attracted considerable interest because of their high enantioselectivity and ability to catalyze a wide variety of transformations under often mild reaction conditions.[1-3] However, the rational design of improved versions of these reactions remains a challenge due to our incomplete understanding of the sundry factors that underlie their activity and stereoselectivity. Computations can provide key insights into these effects, helping to identify both the origins of stereoselectivity and modes of activation, thereby aiding the design of improved catalysts.[4-27] Seminal computational studies from Himo and co-workers[4, 7] and Goodman *et al*.[4-27] emphasized the importance of analyzing the steric complementary of the reacting substrates with the chiral binding pocket created by substituents flanking the phosphoric acid functionality of these catalysts. This steric-centered approach culminated in 2017 with Reid and Goodman[11] identifying the steric factors essential for enantioselectivity in CPA catalyzed reactions involving imines. However, in a growing number of cases such steric-based stereochemical models fail to adequately explain observed selectivities.

The synthesis of dihydroquinazolinone (DHQZ) derivatives is important due to their broad pharmacological activities,[28-32] and a number of recent studies have reported the stereoselective synthesis of 2,3-DHQZ through metal and metal-free catalyzed reactions.[33-36] For instance, in 2008 List *et al*.[37] published the first successful synthesis of 2,3-DHQZ by applying BINOL-derived phosphoric acids to the reaction of 2-aminobenzamides and aldehydes. This provided a highly enantioselective pathway to 2,3-DHQZs with yields ranging from 73% -93% and *ee*'s from 50-98%. Shortly thereafter, Rueping and co-workers[34] showed similar success with this same BINOL-derived catalyst and in 2012, Tian *et al*.[38] accessed the DHQZ framework from the reaction of 2-aminobenzamides and imines using a BINOL phosphoric acid.

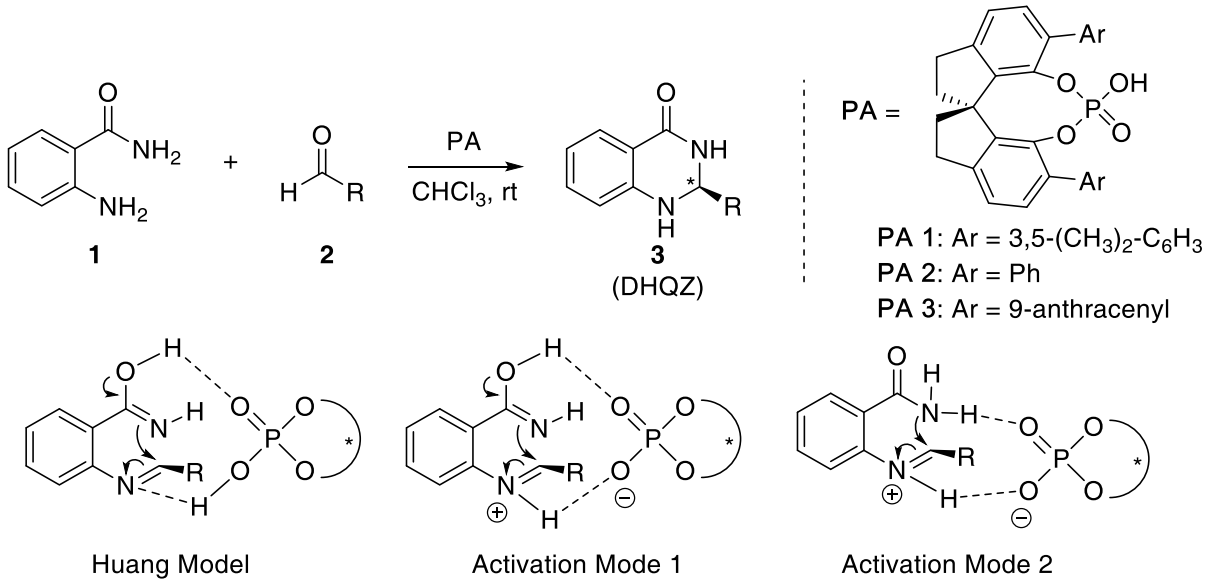

Scheme 1. Phosphoric acid-catalyzed synthesis of 2,3-Dihydroquinazolinones and possible stereocontrolling transition states

In 2013, Huang and co-workers[39] showed that SPINOL-phosophoric acids provides a reliable and efficient method of catalyzing the two-step condensation/amine addition cascade sequence of 2-aminobenzamide and aldehydes to afford the corresponding 2,3-DHQZ (see Scheme 1). They proposed that in the presence of a phosphoric acid (**PA**), the imine intermediate undergoes a stereoselective intramolecular amine addition to afford the final (*S*)-product. Notably, they found that the stereoselectivity is dependent on both the substituents on the catalyst well as those on the phenyl group of the substrate (see Table 1). An initial catalyst screen established that **PA 3** provides a good baseline of stereoselectivity of 88% (Entry 4 of Table 1), with selectivity further tuned by different substituents on the substrate. For instance, Huang *et al*. observed that ortho-substituted benzaladehydes exhibit higher selectivies than either their *m*- and *p*-substituted counterparts or unsubstituted benzaldehyde (see Table 1). Herein, we use density functional theory (DFT) to determine the preferred activation mode for these reactions and to unravel the sundry factors impacting the stereoselectivity.

II. Theoretical Methods

All computations were performed using Gaussian 09[40] using an ultrafine integration grid (99 radial shells and 590 angular points per shell).[41-42] Geometries and harmonic vibrational frequencies were computed at the PCM-B97-D/def2-TZVP level of theory[43-46] with chloroform

as the solvent. Transition state (TS) structures were identified by the presence of a single imaginary vibrational frequency. Free energy thermal corrections were computed with the quasi-RRHO method of Grimme.[47] Final relative free energies are reported at the PCM-B97-D3/def2-TZVP//PCM-B97-D/def2-TZVP level of theory.[48]

III. Results and Discussion

We studied 12 examples of the reaction in Scheme 1 (see Table 1), which involves the condensation of an aromatic aldehyde (**2**) with 2-aminobenzamide (**1**) followed by an intramolecular amidation of the resulting imine. The latter step is stereocontrolling and can proceed from several potential tautomeric states. Huang *et al*.[39] proposed the TS model shown in Scheme 1 in which the acidic functionality of the CPA activates the imine while the phosphoryl oxygen activates the nucleophilic iminol through H-bonding. We find that in the lowest-lying computed TS structure corresponding to this mechanism there is a complete proton transfer from the CPA to the imine and the substrate and catalyst are bound as an ion-pair (Activation Mode 1, Scheme 1). However, exploration of other mechanistic possibilities reveals that the direct activation of the amido form of the substrate is most favorable (Activation Mode 2, Scheme 1), with the rate limiting step lying 8.4 kcal mol^{-1} below that for Activation Mode 1 (for entry 6, see SI Figure S1). As such, our remaining discussion focuses on TS structures corresponding to Activation Mode 2.

Table 1. Experimental enantiomeric excess (ee, %) and $\Delta\Delta G^{\ddagger}$ (kcal mol^{-1}) values and corresponding computational predictions for reaction 1.[a] TS′(E) is favored over TS′(Z) except where noted.

Entry	R	PA	*ee*(exp.)[a]	$\Delta\Delta G^{\ddagger}$(exp.)	*ee*(theor.)	$\Delta\Delta G^{\ddagger}$(theor.)
1[b]	*p*-BrPh	1	23	0.3	12	0.1
2[b]	*p*-BrPh	2	72	1.1	91	1.8
3[b]	*m*-BrPh	3	87	1.6	98	2.7
4	*p*-BrPh	3	88	1.6	99	3.0
5	*p*-OMePh	3	89	1.7	98	2.8
6[b]	Ph	3	90	1.7	95	2.1
7	*m*-OMePh	3	93	2.0	>99	3.2
8	*o*-OMePh	3	94	2.1	>99	4.1
9	*o*-NO_2Ph	3	95	2.2	>99	3.9
10	2,4-Cl_2Ph	3	96	2.3	>99	4.2
11	*o*-ClPh	3	98	2.7	>99	4.2
12	*o*-BrPh	3	98	2.7	>99	4.4

[a] Experimental data from ref [39].
[b] TS′(Z) favored.

In the stereocontrolling intramolecular amidation step, the iminium can exist as either the *E* or *Z* isomer. Each of these can lead to either enantiomer of the final product, giving rise to four fundamental possible TS structures: TS(E) and TS(Z) leading to the favored S-isomer and TS′(Z) and TS′(E) leading to the disfavored R product. We explored low-lying conformations for each of these possible TS structures (see Supporting Information) and then predicted stereoselectivities based on the difference in free energy between the lowest-lying TS structures leading to the two possible stereoisomers ($\Delta\Delta G^{\ddagger}$). Computed *ee* and $\Delta\Delta G^{\ddagger}$ values are listed in Table 1. Despite a systematic overestimation of selectivity derived from the DFT computations, the trend in theoretical $\Delta\Delta G^{\ddagger}$ values are strongly correlated with the experimental data across the range of entries (Figure 1, $r^2 = 0.92$). Importantly, the computational data capture the key trends that **PA 3** is more selective than either **PA 2** or **PA 1** and that o-substituted benzaldehydes exhibit enhanced selectivities compared to p-substituted analogs.

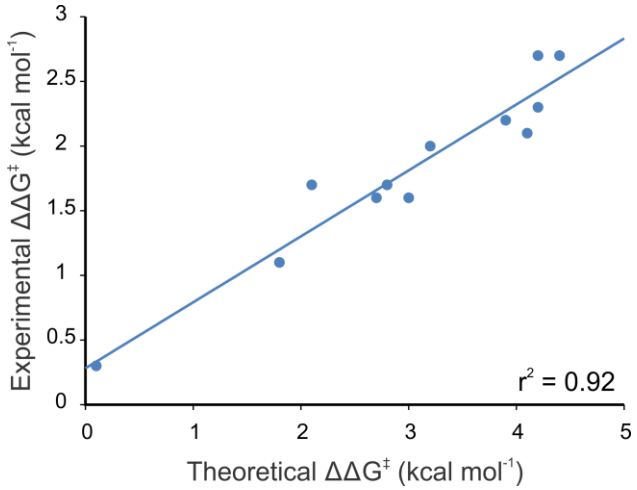

Figure 1. Correlation of experimental vs. theoretical free energy differences between the lowest-lying TS structures leading to the two possible stereoisomers ($\Delta\Delta G^{\ddagger}$)

TS(E), which leads to the favored S product, is always the most favorable TS structure; however, the lowest-lying TS structure leading to the R product varies between the Z and E isomers of the iminium depending on the substrate and catalyst. These three transition states are shown in Figure 2 for R = Ph (Entry 6 of Table 1) as a representative example. TS(E) and TS′(Z) differ primarily in the H and R substituents on the terminal carbon participating in covalent bond breaking/formation. TS(E) and TS′(E) contain mirror images of the substrate and show a marked difference in how the substrate fits within the linear groove created by the anthracenyl groups of the catalyst. One would expect, based on conventional steric-based views

of CPA catalyzed reactions, that TS′(E) should be more favorable than TS(E) (see the "quadrant projection"[4-7] of both structures in Figure 3). Instead, TS(E) is consistently lower in free energy than TS′(E), suggesting that factors other than steric interactions are playing key roles. As seen in Figure 2, these TS structures tend to feature two NH···O hydrogen bonds between the substrate and the phosphate group; however, TS(E) also features a CH···O interaction that will prove important for variations in selectivity depending on the substrate (*vide infra*). Similar CH···O interactions have been observed to play key roles in the selectivity of an increasing number of CPA catalyzed reactions,[12-24] particularly those involving ion-pairs. For example, Duarte and Paton[20] recently found C-H···O interactions to be the dominant short-rage stabilizing feature in a chiral phosphate-mediated desymmetrization of aziridinium and episulfonium cations while Terada and co-workers[24] found similar interactions to be pivotal in a chiral phosphate catalyzed ring expansion of 1,3-dithiane derivatives.

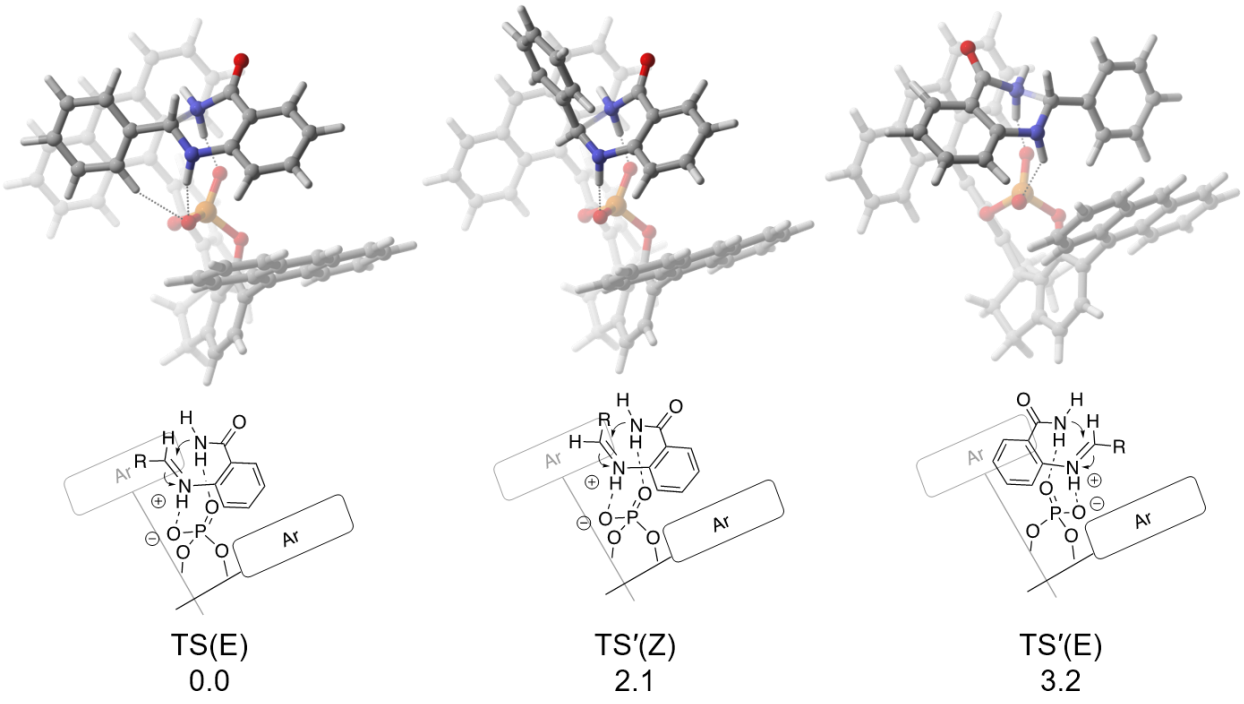

Figure 2. Lowest-lying stereocontrolling TS structures: TS(E), involving the E isomer of the iminium and leading to the S product, and the two competing transition states TS′(Z) and TS′(E), involving the Z and E isomers of the iminium and leading to the R product. R=Ph (Entry 6 of Table 1) is used as a representative example. Relative free energies are shown in kcal mol^{-1}.

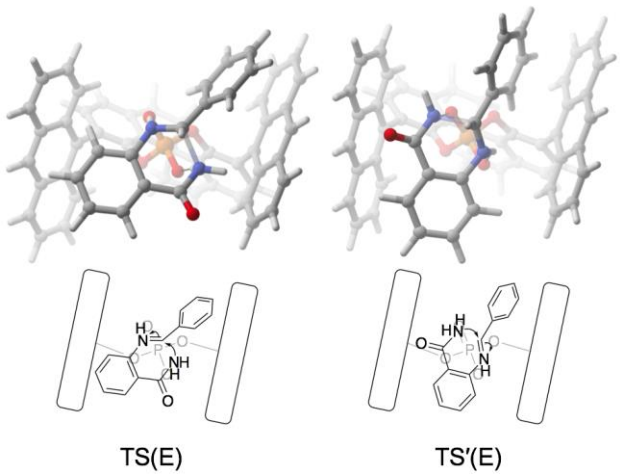

Figure 3. Quadrant projection of TS(E) and TS′(E) for R=Ph.

The computed TS structures allow us to determine why **PA 3** is necessary to achieve at least a modest baseline level of selectivity and why ortho-substituents on the substrate enhance the selectivity. To do this, the gas-phase energy differences ($\Delta\Delta E^{\ddagger}$) between diastereomeric transition states were decomposed into contributions from the distortions of the substrate and catalyst into the TS geometry ($\Delta\Delta E_{sub}$ and $\Delta\Delta E_{cat}$, respectively) and difference in non-covalent interactions between the substrate and catalyst, $\Delta\Delta E_{int}$:[49,50]

$$\Delta\Delta E^{\ddagger} = \Delta\Delta E_{sub} + \Delta\Delta E_{cat} + \Delta\Delta E_{int}$$

These quantities are given in Table 2 for the lowest-lying (*R*)-transition state [either TS′(Z) or TS′(E)] relative to TS(E), for selected entries from Table 1.

Table 2. Solution-phase $\Delta\Delta G^{\ddagger}$ and gas-phase $\Delta\Delta E^{\ddagger}$, $\Delta\Delta E_{cat}$, $\Delta\Delta E_{sub}$, and $\Delta\Delta E_{int}$ values for selected entries from Table 1 as well as $\Delta\Delta E_{int}$ for M1-M4, in kcal mol^{-1}.

Entry	$\Delta\Delta G^{\ddagger}$	$\Delta\Delta E^{\ddagger}$	$\Delta\Delta E_{cat}$	$\Delta\Delta E_{sub}$	$\Delta\Delta E_{int}$	$\Delta\Delta E_{int}$(M1)	$\Delta\Delta E_{int}$(M2)	$\Delta\Delta E_{int}$(M3)	$\Delta\Delta E_{int}$(M4)
1	0.1[a]	1.5	-1.0	1.3	1.2	0.2	1.0	0.0	-0.5
4	3.0[b]	3.5	-0.2	1.1	2.6	-1.0	5.6	1.9	1.8
6	2.1[a]	4.1	-0.2	2.0	2.2	0.6	2.3	0.6	0.0
6	3.2[b]	3.9	-0.3	1.1	3.1	-0.5	5.9	2.3	2.1
9	3.9[b]	4.1	-0.3	1.2	3.1	-1.7	7.5	2.6	2.4
10	4.2[b]	4.1	-0.1	0.8	3.4	-1.7	8.2	3.1	3.1
11	4.2[b]	4.4	-0.3	1.0	3.7	-0.3	7.4	3.3	3.2
12	4.4[b]	4.6	-0.2	1.1	3.8	-0.4	7.7	3.5	3.3

[a] Differences between TS′(Z) and TS(E)
[b] Differences between TS′(E) and TS(E)

With the exception of Entry 1, the contribution of the catalyst distortion energy to $\Delta\Delta E^{\ddagger}$, $\Delta\Delta E_{cat}$, is uniformly small (-0.2 ± 0.1 kcal mol^{-1}). The contribution of substrate distortion energy ($\Delta\Delta E_{sub}$), on the other hand, varies from 0.0 to 2.5 kcal mol^{-1} while $\Delta\Delta E_{int}$ ranges from 1.2 to 3.8 kcal mol^{-1}. Thus, differences in the non-covalent interactions between the substrate and catalyst ($\Delta\Delta E_{int}$) are the dominant factor in controlling stereoselectivity of these reactions. This is compatible with the now common observation that differential non-covalent interactions are a potent driving force in the stereoselectivity of CPA catalysis.[51-52] To further quantify approximate contributions to $\Delta\Delta E_{int}$ arising from interactions of the substrate with specific components of the catalyst, $\Delta\Delta E_{int}$ values were computed for a series of truncated models (M1-M4 in Figure 4).[9] For each of these models, one or more fragments of the catalyst were removed and replaced with a hydrogen atom that was optimized while keeping all other atoms fixed. In M1, one of the aryl substituents is removed from the catalyst; in M2, the opposing substituent is removed. In M3, both aryl substituents are removed while M4 is a version of M3 with the SPINOL backbone removed and the (deprotonated) catalyst reduced to the core phosphate group.

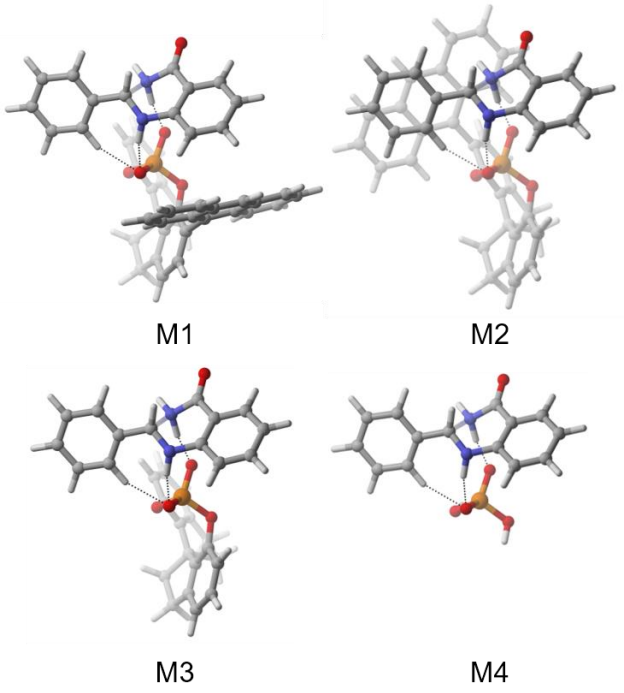

Figure 4. Truncated models M1-M4 used to localize contributions to $\Delta\Delta E_{int}$. TS(E) for the R=Ph case (Entry 6 of Table 1) is used here as a representative example.

Entry 1, with **PA 1**, exhibits poor selectivity experimentally (ee = 23%) and the computed free energy difference ($\Delta\Delta G^{\ddagger}$ = 0.1 kcal mol^{-1}) leads to a theoretical *ee* (12%) in close

agreement. However, the underlying gas-phase energy difference ($\Delta\Delta E^{\ddagger}$) is 1.5 kcal mol^{-1}, indicating that entropy and solvent effects drastically reduce the selectivity in this case. With regard to the contributions to $\Delta\Delta E^{\ddagger}$, the catalyst and substrate distortion energies nearly cancel, so the bulk of the 1.5 kcal mol^{-1} energy difference arises from the $\Delta\Delta E_{int}$ value of 1.2 kcal mol^{-1}. This is reduced to 0.0 and -0.5 kcal mol^{-1}, respectively, for $\Delta\Delta E_{int}$(M3) and $\Delta\Delta E_{int}$(M4), implying that the modest $\Delta\Delta E_{int}$ value arises chiefly from interactions of the substrate with the aryl substituents on the catalyst. This is apparent in the corresponding TS structures; in TS(E), the phenyl substituent at the carbon undergoing bond breaking/formation is positioned to engage in CH/π interactions with the nearby 3,5-$(CH_3)_2$-C_6H_2, whereas in TS′(Z) these interactions are absent. This is reflected in the $\Delta\Delta E_{int}$(M2) value of 1.0 kcal mol^{-1}.

For entry 4, which features the same substrate as entry 1 but uses **PA 3** as catalyst, the selectivity is markedly higher. This is reproduced computationally, with $\Delta\Delta G^{\ddagger}$ and $\Delta\Delta E^{\ddagger}$ values of 3.0 and 3.5 kcal mol^{-1}, respectively. The larger $\Delta\Delta E^{\ddagger}$ value for entry 4, versus 1, is due to the decrease in magnitude of $\Delta\Delta E_{cat}$ and increase in $\Delta\Delta E_{int}$. As with entry 1, the latter effect can be traced to stabilizing π-stacking interactions between the substrate and the nearby aryl substituent on the catalyst in TS(E), as captured by $\Delta\Delta E_{int}$(M2). However, the stacking interaction with the anthracenyl group of **PA 3** is stronger than with the 3,5-$(CH_3)_2$-C_6H_2 group in **PA 1**, leading to the enhanced selectivity of **PA 3**. This effect is even stronger for entry 9 (R=*o*-NO_2Ph), presumably due to the well-established ability of nitro substituents to enhance π-stacking interactions,[53-55] and slightly weaker for the unsubstituted substrate (entry 6).

For entries 10-12, with *o*-halogenated benzaldehydes, TS′(Z) does not exhibit the dual NH···O hydrogen bonding configuration with the catalyst observed in other cases and shown in Figure 2. This is because the iminium functionality is displaced due to a repulsive steric interaction between the catalyst and the ortho substituent [see TS′ (Z) in Figure 5 for R=*o*-BrPh]. The result is that TS′ (E) is the favored (*R*)-transition state structure for these entries. A note of interest is that the substituents on the phenyl group of the substrate in TS′(E) are always oriented away from and do not interact directly with the phosphate oxygens. In all three cases, $\Delta\Delta E_{cat}$ is negligible and $\Delta\Delta E_{sub}$ is relatively constant and similar to that for entry 4. Thus, $\Delta\Delta E_{int}$ appears to be responsible for the impact of o-substitution on the stereoselectivity of these reactions. Moreover, the trend in $\Delta\Delta E_{int}$ values is retained in M4, indicating that the effect of o-substituents is due to non-covalent interactions between the substrate and the phosphate core of the catalyst.

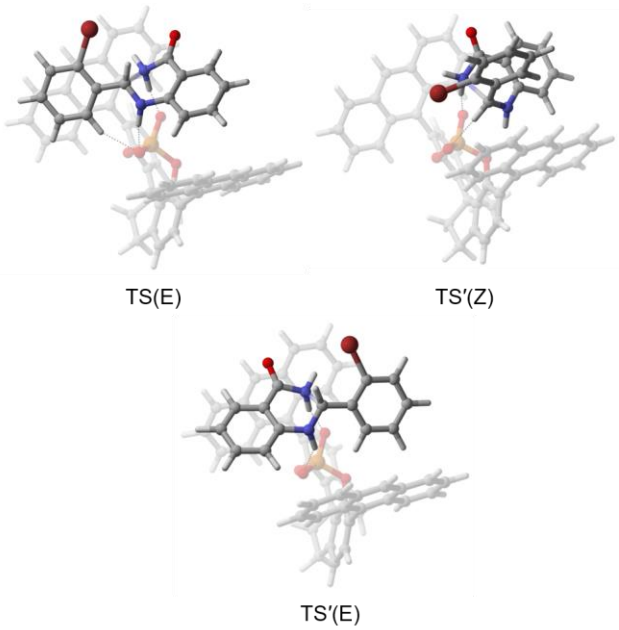

Figure 5. TS(E), TS′ (Z) and TS′ (E) for entry 12 of Table 1.

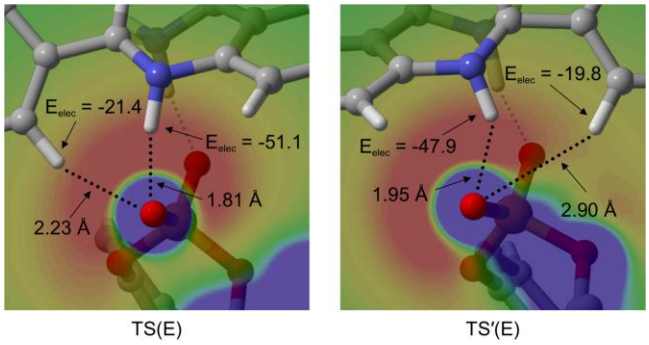

Figure 6. Electrostatic potential, in the absence of the substrate, in the plane of the oxygen and hydrogen atoms of the critical CH···O and NH···O interactions in TS(E) and TS′ (E) (blue = 0.0 kcal mol^{-1}; red = -125.5 kcal mol^{-1}). The R=Ph case is shown.

To understand this effect, we can take the energy differences between TS′(E) and TS(E) for entry 6, with R = Ph, as a baseline. In this case, the $\Delta\Delta E_{int}$(M4) value of 2.1 kcal mol^{-1} is consistently 1 kcal mol^{-1} smaller than for entries 10-12. This can be attributed to changes in the strength of the NH···O and CH···O interactions. These, in turn, can be analyzed in terms of the interaction of the proton with the electrostatic potential (ESP) created by the catalyst, as done recently by Maji and Wheeler[56] in their analyses of NHC-catalyzed kinetic resolutions. For instance, Figure 6 shows the ESP of the catalyst in the plane of the CH and NH bonds for TS(E) and TS′(E) for entry 6, along with the atomic charges on the hydrogens and resulting electrostatic

interaction (E_{elec}). The difference in E_{elec} for the NH···O and CH···O interactions in this case are 3.2 and 1.6 kcal mol^{-1}, respectively, favoring TS(E). In other words, the NH···O and CH···O interactions are electrostatically more favorable in TS(E) than in TS′ (E), as depicted in Figure 7. This difference in H-bond strength is also reflected in the geometries, with TS(E) exhibiting shorter XH···O distances and more linear XHO angles.

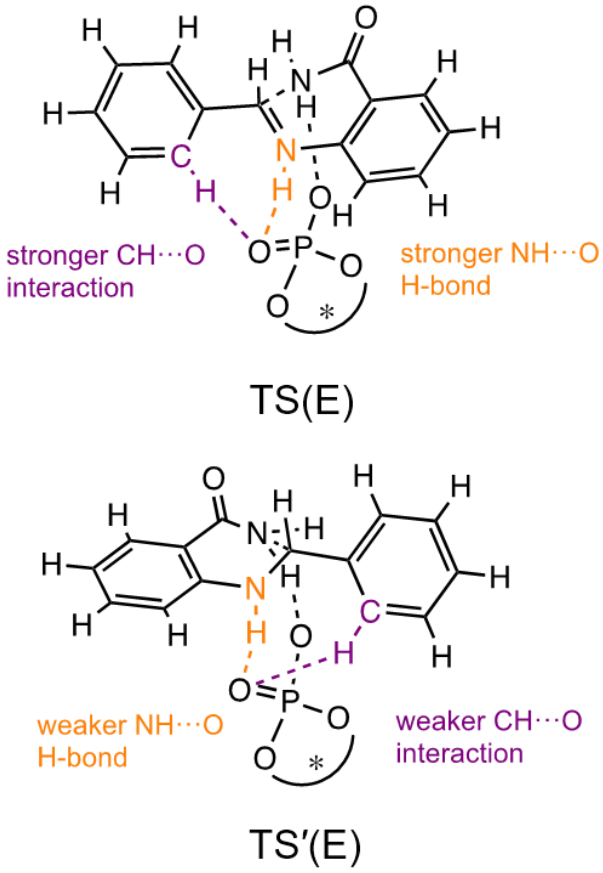

Figure 7. Key electrostatic interactions differentiating the TS(E) and TS′ (E) structures.

The analogous data for entries 10-12 is listed in Table 3. These data show the same effect observed for entry 6 but with larger magnitudes. More precisely, the introduction of *o*-substituents leads to an enhancement of the strength of the NH···O and CH···O interactions in TS(E), but not in TS′(E). This can be seen both in terms of the electrostatic analysis and the geometries. The modulations of the NH···O interaction is the more dominant effect, with the CH···O interaction playing a smaller, yet also significant, role. Thus, while the anthracenyl substituents in **PA3** area clearly vital for stereoselectivity, it is variations in the XH···O

interactions involving the phosphoric acid core of the catalyst that lead to the changes observed for different substrates.

Table 3. Charge of and ESP (kcal mol^{-1}) experienced by the hydrogen in the stereocontrolling XH···O interactions (X = N or C) of TS(E) and TS'(E) for selected entries of Table 1, along with the corresponding electrostatic energy E_{elec} (kcal mol^{-1}), XH···O interaction distance (Å), XHO angle (degrees), and difference in electrostatic energy ΔE_{elec} (kcal mol^{-1}).

	TS(E)					TS'(E)					
Entry	*q*(H)	ESP(H)	E_{elec}	XH···O length	XHO angle	*q*(H)	ESP(H)	E_{elec}	XH···O length	XHO angle	ΔE_{elec}
					NH···O						
6	0.405	-126.3	-51.1	1.81	161.4	0.400	-119.8	-47.9	1.95	141.0	3.2
10	0.402	-128.8	-51.7	1.77	164.0	0.396	-119.9	-47.5	1.97	144.4	4.2
11	0.403	-128.5	-51.7	1.77	164.3	0.397	-120.5	-47.9	1.95	144.4	3.9
12	0.402	-128.6	-51.7	1.77	164.4	0.397	-119.8	-47.6	1.97	144.2	4.1
					CH···O						
6	0.201	-106.4	-21.4	2.23	158.6	0.203	-97.4	-19.8	2.90	145.6	1.6
10	0.209	-106.9	-22.4	2.20	157.2	0.214	-95.2	-20.4	3.02	136.8	2.0
11	0.204	-106.4	-21.6	2.22	155.6	0.209	-95.4	-20.0	2.98	138.5	1.7
12	0.205	-106.7	-21.9	2.21	155.9	0.210	-95.1	-19.9	3.01	137.7	2.0

IV. Conclusions

The selectivity of the SPINOL phosphoric acid catalyzed synthesis of 2,3-dihydroquinazolinones (Scheme 1) depends on both the catalyst and substrate, confounding attempts to unravel the origin of these stereoselectivity changes through experiment alone. We have examined a dozen examples of this reaction using DFT, showing good agreement between computed selectivities and experimental data. Computations reveal that the preferred activation mode for this transformation involves the amide tautomer of an iminium ion intermediate undergoing intramolecular amine addition. In most cases, this is stabilized by two NH···O interactions with the catalyst. Examination of the key stereocontrolling TS structures show that **PA 3**, featuring 9-nathracenyl substituents, achieves selectivity through a combination of stabilizing π-stacking interactions of the substrates with the aryl substituents and NH···O and CH···O interactions between the substrate and phosphoric acid core of the catalyst. The former are impacted by substituent effects on π-stacking interactions whereas the latter are perturbed in a subtle way in the case of ortho-substituted benzaldehydes, leading to the observed enhanced selectivity.

BINOL and SPINOL derived phosphoric acid catalyzed transformations have been extensively studied both experimentally and computationally[4-27] and the importance of both repulsive (steric) and attractive non-covalent interactions between the substrate and the substituents on the catalysts is now widely appreciated. However, as seen above, non-covalent NH···O and CH···O between the substrate and the phosphoric acid core of these catalysts can also prove pivotal, particularly in explaining variations in selectivity with different substrates. Moreover, the strength of these interactions is modulated by the electrostatic potential arising from the phosphoric acid. Similar electrostatically-modulated variations in the strength of XH···O interactions are likely impacting the selectivity of other CPA catalyzed transformations, adding a new layer of complexity to our understanding of these reactions and a new avenue along which their performance can be enhanced.

Supporting Information Available: Additional Figures, computational details, energies, Cartesian coordinates. This information is available free of charge on the ACS Publications website.

Acknowledgments

This work was supported by National Science Foundation (Grants CHE-1665407 and CHE-1359175). Portions of this research were conducted using high performance research computing resources provided by Texas A&M University (http://hprc.tamu.edu).

References

1. Akiyama, T., Stronger bronsted acids. *Chem. Rev.* **2007,** *107* (12), 5744-5758.
2. Kampen, D.; Reisinger, C. M.; List, B., Chiral bronsted acids for asymmetric organocatalysis. In *Asymmetric organocatalysis*, List, B., Ed. Springer-Verlag Berlin: Berlin, 2009; Vol. 291, pp 395-456.
3. Parmar, D.; Sugiono, E.; Raja, S.; Rueping, M., Complete field guide to asymmetric binol-phosphate derived bronsted acid and metal catalysis: History and classification by mode of activation; bronsted acidity, hydrogen bonding, ion pairing, and metal phosphates. *Chem. Rev.* **2014,** *114* (18), 9047-9153.
4. Marcelli, T.; Hammar, P.; Himo, F., Phosphoric acid catalyzed enantioselective transfer hydrogenation of imines: A density functional theory study of reaction mechanism and the origins of enantioselectivity. *Chemistry* **2008,** *14* (28), 8562-8571.
5. Simon, L.; Goodman, J. M., Theoretical study of the mechanism of hantzsch ester hydrogenation of imines catalyzed by chiral binol-phosphoric acids. *J Am Chem Soc* **2008,** *130* (27), 8741-8747.
6. Simon, L.; Goodman, J. M., Mechanism of binol--phosphoric acid-catalyzed strecker reaction of benzyl imines. *J Am Chem Soc* **2009,** *131* (11), 4070-4077.
7. Marcelli, T.; Hammar, P.; Himo, F., Origin of enantioselectivity in the organocatalytic reductive amination of α-branched aldehydes. *Advanced Synthesis & Catalysis* **2009,** *351* (4), 525-529.
8. Simón, L.; Goodman, J. M., Dft study on the factors determining the enantioselectivity of friedel−crafts reactions of indole with n-acyl and n-tosylimines catalyzed by binol−phosphoric acid derivatives. *J. Org. Chem.* **2010,** *75* (3), 589-597.
9. Seguin, T. J.; Wheeler, S. E., Competing noncovalent interactions control the stereoselectivity of chiral phosphoric acid catalyzed ring openings of 3-substituted oxetanes. *ACS Catal.* **2016,** *6* (10), 7222-7228.
10. Reid, J. P.; Simon, L.; Goodman, J. M., A practical guide for predicting the stereochemistry of bifunctional phosphoric acid catalyzed reactions of imines. *Acc Chem Res* **2016,** *49* (5), 1029-1041.
11. Reid, J. P.; Goodman, J. M., Selecting chiral binol-derived phosphoric acid catalysts: General model to identify steric features essential for enantioselectivity. *Chemistry* **2017,** *23* (57), 14248-14260.
12. Grayson, M. N.; Pellegrinet, S. C.; Goodman, J. M., Mechanistic insights into the binol-derived phosphoric acid-catalyzed asymmetric allylboration of aldehydes. *J. Am. Chem. Soc.* **2012,** *134* (5), 2716-2722.
13. Grayson, M. N.; Goodman, J. M., Understanding the mechanism of the asymmetric propargylation of aldehydes promoted by 1,1'-bi-2-naphthol-derived catalysts. *J. Am. Chem. Soc.* **2013,** *135* (16), 6142-6148.
14. Grayson, M. N.; Goodman, J. M., Lewis acid catalysis and ligand exchange in the asymmetric binaphthol-catalyzed propargylation of ketones. *J. Org. Chem.* **2013,** *78* (17), 8796-8801.
15. Grayson, M. N.; Krische, M. J.; Houk, K. N., Ruthenium-catalyzed asymmetric hydrohydroxyalkylation of butadiene: The role of the formyl hydrogen bond in stereochemical control. *J. Am. Chem. Soc.* **2015,** *137* (27), 8838-8850.

16. Overvoorde, L. M.; Grayson, M. N.; Luo, Y.; Goodman, J. M., Mechanistic insights into a binol-derived phosphoric acid-catalyzed asymmetric pictet-spengler reaction. *J. Org. Chem.* **2015,** *80* (5), 2634-2640.
17. Takagi, R.; Nishi, T., Organocatalytic asymmetric desymmetrization of 4,4-disubstituted cyclohexadienones via an intermolecular diels-alder reaction. *Org Biomol Chem* **2015,** *13* (45), 11039-11045.
18. Kondoh, A.; Ota, Y.; Komuro, T.; Egawa, F.; Kanomata, K.; Terada, M., Chiral bronsted acid-catalyzed enantioselective friedel-crafts reaction of 2-methoxyfuran with aliphatic ketimines generated in situ. *Chem Sci* **2016,** *7* (2), 1057-1062.
19. Grayson, M. N.; Yang, Z.; Houk, K. N., Chronology of ch...O hydrogen bonding from molecular dynamics studies of the phosphoric acid-catalyzed allylboration of benzaldehyde. *J. Am. Chem. Soc.* **2017,** *139* (23), 7717-7720.
20. Duarte, F.; Paton, R. S., Molecular recognition in asymmetric counteranion catalysis: Understanding chiral phosphate-mediated desymmetrization. *J Am Chem Soc* **2017,** *139* (26), 8886-8896.
21. Maji, R.; Champagne, P. A.; Houk, K. N.; Wheeler, S. E., Activation mode and origin of selectivity in chiral phosphoric acid-catalyzed oxacycle formation by intramolecular oxetane desymmetrizations. *ACS Catal.* **2017,** *7* (10), 7332-7339.
22. Falcone, B. N.; Grayson, M. N.; Rodriguez, J. B., Mechanistic insights into a chiral phosphoric acid-catalyzed asymmetric pinacol rearrangement. *J. Org. Chem.* **2018,** *83* (23), 14683-14687.
23. Wang, M.; Khan, S.; Miliordos, E.; Chen, M., Enantioselective allenylation of aldehydes via brønsted acid catalysis. *Advanced Synthesis & Catalysis* **2018,** *360* (23), 4634-4639.
24. Li, F.; Korenaga, T.; Nakanishi, T.; Kikuchi, J.; Terada, M., Chiral phosphoric acid catalyzed enantioselective ring expansion reaction of 1,3-dithiane derivatives: Case study of the nature of ion-pairing interaction. *J Am Chem Soc* **2018,** *140* (7), 2629-2642.
25. Maji, R.; Mallojjala, S. C.; Wheeler, S. E., Chiral phosphoric acid catalysis: From numbers to insights. *Chem. Soc. Rev.* **2018,** *47* (4), 1142-1158.
26. Maji, R.; Mallojjala, S. C.; Wheeler, S. E., Chiral phosphoric acid catalysis: From numbers to insights. *Chemical Society Reviews* **2018,** *47* (4), 1142-1158.
27. Reid, J. P.; Sigman, M. S., Holistic prediction of enantioselectivity in asymmetric catalysis. *Nature* **2019,** *571* (7765), 343-348.
28. Bonola, G.; Dare, P.; Magistre.Mj; Massaran.E; Setnikar, I., 1-aminoacyl-2,3-dihydro-4(1h)-quinazolinone derivatives with choleretic and antifibrillatory activity. *J. Med. Chem.* **1968,** *11* (6), 1136-&.
29. Chinigo, G. M.; Paige, M.; Grindrod, S.; Hamel, E.; Dakshanamurthy, S.; Chruszcz, M.; Minor, W.; Brown, M. L., Asymmetric synthesis of 2,3-dihydro-2-arylquinazolin-4-ones: Methodology and application to a potent fluorescent tubulin inhibitor with anticancer activity. *J. Med. Chem.* **2008,** *51* (15), 4620-4631.
30. Levin, J. I.; Chan, P. S.; Bailey, T.; Katocs, A. S.; Venkatesan, A. M., The synthesis of 2,3-dihydro-4(1h)-quinazolinone angiotensin-ii receptor antagonists. *Bioorg. Med. Chem. Lett.* **1994,** *4* (9), 1141-1146.
31. Okumura, K.; Oine, T.; Yamada, Y.; Hayashi, G.; Nakama, M., 4-oxo-1,2,3,4-tetrahydroquinazolines .I. Syntheses and pharmacological properties of 2-methyl-3-aryl-4-oxo-1,2,3,4-tetrahydroquinazolines and their 1-acyl derivatives. *J. Med. Chem.* **1968,** *11* (2), 348-&.

32. Uzunov, D. P.; Zivkovich, I.; Pirkle, W. H.; Costa, E.; Guidotti, A., Enantiomeric resolution with a new chiral stationary-phase of 7-chloro-3-methyl-3,4-dihydro-2h-1,2,4-benzothiadiazine s,s-dioxide, a cognition-enhancing benzothiadiazine derivative. *J. Pharm. Sci.* **1995,** *84* (8), 937-942.
33. Prakash, M.; Kesavan, V., Highly enantioselective synthesis of 2,3-dihydroquinazolinones through intramolecular amidation of imines. *Org. Lett.* **2012,** *14* (7), 1896-1899.
34. Rueping, M.; Antonchick, A. P.; Sugiono, E.; Grenader, K., Asymmetric bronsted acid catalysis: Catalytic enantioselective synthesis of highly biologically active dihydroquinazolinones. *Angewandte Chemie-International Edition* **2009,** *48* (5), 908-910.
35. Wu, J.; Du, X. L.; Ma, J.; Zhang, Y. P.; Shi, Q. C.; Luo, L. J.; Song, B. A.; Yang, S.; Hu, D. Y., Preparation of 2,3-dihydroquinazolin-4(1h)-one derivatives in aqueous media with beta-cyclodextrin-so3h as a recyclable catalyst. *Green Chem.* **2014,** *16* (6), 3210-3217.
36. Saito, K. M., Y. Akiyama, T., Chiral phosphoric acid catalyzed asymmetric synthesis of 2-substituted 2,3-dihydro-4-quinolones by a protecting-group-free approach. *Org. Lett.* **2015,** *17* (13), 3203-3205.
37. Cheng, X.; Vellalath, S.; Goddard, R.; List, B., Direct catalytic asymmetric synthesis of cyclic aminals from aldehydes. *J. Am. Chem. Soc.* **2008,** *130* (47), 15786-+.
38. Cheng, D. J.; Tian, Y.; Tian, S. K., Catalytic asymmetric synthesis of dihydroquinazolinones from imines and 2-aminobenzamides. *Adv. Synth. Catal.* **2012,** *354* (6), 995-999.
39. Huang, D.; Li, X.; Xu, F.; Li, L.; Lin, X., Highly enantioselective synthesis of dihydroquinazolinones catalyzed by spinol-phosphoric acids. *ACS Catal.* **2013,** *3* (10), 2244-2247.
40. Frisch, M. J. T., G. W.; Schlegel, H. B.; Scuseria, G. E.; Robb, M. A.; Cheeseman, J. R.; Scalmani, G.; Barone, V.; Mennucci, B.; Petersson, G. A.; Nakatsuji, H.; Caricato, M.; Li, X.; Hratchian, H. P.; Izmaylov, A. F.; Bloino, J.; Zheng, G.; Sonnenberg, J. L.; Hada, M.; Ehara, M.; Toyota, K.; Fukuda, R.; Hasegawa, J.; Ishida, M.; Nakajima, T.; Honda, Y.; Kitao, O.; Nakai, H.; Vreven, T.; Montgomery, J. A., Jr.; Peralta, J. E.; Ogliaro, F.; Bearpark, M.; Heyd, J. J.; Brothers, E.; Kudin, K. N.; Staroverov, V. N.; Kobayashi, R.; Normand, J.; Raghavachari, K.; Rendell, A.; Burant, J. C.; Iyengar, S. S.; Tomasi, J.; Cossi, M.; Rega, N.; Millam, N. J.; Klene, M.; Knox, J. E.; Cross, J. B.; Bakken, V.; Adamo, C.; Jaramillo, J.; Gomperts, R.; Stratmann, R. E.; Yazyev, O.; Austin, A. J.; Cammi, R.; Pomelli, C.; Ochterski, J. W.; Martin, R. L.; Morokuma, K.; Zakrzewski, V. G.; Voth, G. A.; Salvador, P.; Dannenberg, J. J.; Dapprich, S.; Daniels, A. D.; Farkas, Ö.; Foresman, J. B.; Ortiz, J. V.; Cioslowski, J.; Fox, D. J. Gaussian 09, Revision D.01; Gaussian, Inc., Wallingford, CT, 2009.
41. Wheeler, S. E.; Houk, K. N., Integration grid errors for meta-gga-predicted reaction energies: Origin of grid errors for the m06 suite of functionals. *J. Chem. Theory Comput.* **2010,** *6* (2), 395-404.
42. Bootsma, A. N.; Wheeler, S. E., Popular integration grids can result in large errors in dft-computed free energies. *ChemRxiv, DOI: 10.26434/chemrxiv.8864204.v5*.
43. Tomasi, J.; Mennucci, B.; Cammi, R., Quantum mechanical continuum solvation models. *Chem. Rev.* **2005,** *105* (8), 2999-3094.
44. Miertuš, S.; Scrocco, E.; Tomasi, J., Electrostatic interaction of a solute with a continuum. A direct utilizaion of ab initio molecular potentials for the prevision of solvent effects. *Chem. Phys.* **1981,** *55* (1), 117-129.

45. Grimme, S., Semiempirical gga-type density functional constructed with a long-range dispersion correction. *J. Comput. Chem.* **2006,** *27* (15), 1787-1799.
46. Weigend, F.; Ahlrichs, R., Balanced basis sets of split valence, triple zeta valence and quadruple zeta valence quality for h to rn: Design and assessment of accuracy. *Phys. Chem. Chem. Phys.* **2005,** *7* (18), 3297-3305.
47. Grimme, S., Supramolecular binding thermodynamics by dispersion-corrected density functional theory. *Chem. Eur. J.* **2012,** *18* (32), 9955-9964.
48. Grimme, S.; Antony, J.; Ehrlich, S.; Krieg, H., A consistent and accurate ab initio parametrization of density functional dispersion correction (dft-d) for the 94 elements h-pu. *J. Chem. Phys.* **2010,** *132* (15), 154104.
49. Ess, D. H.; Houk, K. N., Distortion/interaction energy control of 1,3-dipolar cycloaddition reactivity. *J. Am. Chem. Soc.* **2007,** *129* (35), 10646-10647.
50. Note that the interaction energy in this case arises from non-covalent interactions between the reacting substrate and the catalyst, not due to the interaction of the reacting fragments as in traditional distortion-interaction analyses of bimolecular reactions. As such, the present analysis will be insensitive to the position of the TS structures along the reaction coordinate (i.e. early vs late TS).
51. Knowles, R. R.; Jacobsen, E. N., Attractive noncovalent interactions in asymmetric catalysis: Links between enzymes and small molecule catalysts. *Proc. Natl. Acad. Sci. USA* **2010,** *107*, 20678-20685.
52. Wheeler, S. E.; Seguin, T. J.; Guan, Y.; Doney, A. C., Noncovalent interactions in organocatalysis and the prospect of computational catalyst design. *Acc. Chem. Res.* **2016,** *49* (5), 1061-1069.
53. Raju, R. K.; Bloom, J. W. G.; An, Y.; Wheeler, S. E., Substituent effects in non-covalent interactions with aromatic rings: Insights from computational chemistry. *ChemPhysChem* **2011,** *12*, 3116-3130.
54. Wheeler, S. E., Understanding substituent effects in non-covalent interactions involving aromatic rings. *Acc. Chem. Res.* **2013,** *46*, 1029-1038.
55. Wheeler, S. E.; Bloom, J. W. G., Toward a more complete understanding of non-covalent interactions involving aromatic rings. *J. Phys. Chem. A* **2014,** *118*, 6133-6147.
56. Maji, R.; Wheeler, S. E., Importance of electrostatic effects in the stereoselectivity of nhc-catalyzed kinetic resolutions. *J. Am. Chem. Soc.* **2017,** *139* (36), 12441-12449.

TOC Figure